INT. J. NUM. METH. HEAT FLUID FLOW, VOL. 2, 235–242 (1992)

NUMERICAL STUDY OF A PURE METAL MELTING IN PRESENCE OF TURBULENT NATURAL CONVECTION

YONGKE WU

Département des Sciences Appliquées, Université du Québec à Chicoutimi, Chicoutimi, Québec, G7H 2B1, Canada

AND

MARCEL LACROIX

Département de Génie Mécanique, Université de Sherbrooke, Sherbrooke, Québec, J1K 2R1, Canada

ABSTRACT

Melting of pure metal in presence of turbulent natural convection with Rayleigh number ranging from 10^6 to 10^9 has been studied numerically. The governing equations are formulated in terms of stream function–vorticity–temperature and the moving distorted solid/liquid interface is tracked using body-fitted coordinates. The turbulent flow is taken into account using an algebraic eddy-viscosity model with Prandtl's mixing length. Results indicate that turbulent natural convection plays a more significant role than laminar flow in the process of melting. Heat transfer and melting rates are significantly increased and a correlation for the average Nusselt number at the heated wall in the quasi-steady melting regime is proposed.

KEY WORDS Metal melting Turbulent natural convection

NOMENCLATURE

c	specific heat of liquid
H	height of the cavity
$g^{i,j}$	geometric coefficients in (2)
Δh	latent heat of fusion
l	Prandtl's mixing length
L	width of the cavity
m	general coefficient in (1)
$\underline{Nu}$	local Nusselt number
$\overline{Nu}$	average Nusselt number
Pr	Prandtl number (ν_l/α_l)
Ra	Rayleigh number $[g\beta(T_w-T_f)H^3/\nu\alpha]$
S	source term in (1)
Ste	Stefan number $[c(T_w-T_f)/\Delta h]$
t	dimensionless time $(t^*\alpha_l/H)$
T_f	fusion temperature
T_w	temperature of the heated wall
U	contravariant velocity in ξ direction
V	contravariant velocity in η direction
V_f	molten volume reaction
x	dimensionless coordinate (x^*/H)
y	dimensionless coordinate (y^*/H)
α	thermal diffusivity
ε_M	eddy viscosity (ν_t/α_l)
ε_H	eddy viscosity of heat
θ	dimensionless temperature $[(T-T_f)/(T_w-T_f)]$
ω	vorticity $(\partial v/\partial x-\partial u/\partial y)$
ψ	stream function
ν	kinematic viscosity
ξ	transformed coordinate
η	transformed coordinate
$\tilde{\rho}$	ratio ρ_s/ρ_l
ρ	general coefficient in (1)
Γ	general coefficient in (1)
ϕ	general dependent variable

Superscript

*	indicates dimension quantities

Subscript

l	liquid
f	fusion point
w	heated wall

0961–5539/92/030235–08$2.00

Received July 1991
Revised January 1992

INTRODUCTION

Melting and solidification of metals is of particular interest in material processing, metallurgy, purification of metals, solidification of castings and ingots and various other solidification technologies. While undergoing phase change, the associated density gradients in a gravitational field can induce natural convection flows in the liquid phase. It has been shown experimentally[1] and later confirmed by numerical studies[2–5] that natural convection can considerably affect the solid/liquid interface shape and motion during phase change.

Over the last decade, the problem of natural convection dominated melting of low Prandtl number substances in enclosures has received increasing research attention. Several authors have conducted successfully numerical simulations of this process. Morgan[2] appears to be one of the first authors to report on a numerical analysis of freezing and melting with convection. An explicit finite element method was used to study the influence of natural convection on the process of freezing and melting in a cylindrical cavity. A fixed grid enthalpy method was employed for the phase change problem. On the other hand, Webb *et al.*[3] have reported one of the first studies on the problem of melting of a pure metal (low Prandtl number) inside a rectangular cavity. A control volume-based discretization scheme adapted for irregular geometries was employed. Brent *et al.*[4] have tackled the same problem using a fixed grid enthalpy-porosity approach. Then, Lacroix[8] solved the problem by invoking a Eulerian–Lagrangian transformation technique.

In all these numerical studies, however, the convection flow was assumed to be laminar. For practical applications, melting and solidification of metals usually involved natural convection flows that are turbulent. As a result, during melting, turbulent natural convection increases even more the overall transport rate and hence the growth rate of the liquid phase.

The purpose of the present study is twofold: First, a computational methodology is presented for the simulation of melting of a pure metal from an isothermal vertical wall driven by turbulent natural convection in the melt. Second, through a series of numerical experiments, the model is then used to examine the effect of turbulent flow in the melt on the motion and the shape of the solid/liquid interface and the overall heat transfer rate.

PHYSICAL MODEL AND GOVERNING EQUATIONS

The phase change material (PCM) is contained in a two-dimensional rectangular cavity of height H and width L (*Figure 1*)

The PCM is assumed to be initially at its fusion temperature T_f, eliminating the need for solution of the energy equation in the solid. At time $t=0$, the temperature of the left vertical wall is raised impulsively to a prescribed temperature above the fusion point, $T_w > T_f$. The horizontal walls connecting the heated wall and the solid/liquid interface are adiabatic. All walls form hydrodynamically no-slip boundary conditions. It is assumed that the thermophysical properties are constant. The Boussinesq approximation is valid; i.e., liquid density variations arise only in the buoyancy source term, but are otherwise neglected. Viscous dissipation is neglected. The liquid is Newtonian and incompressible and the flow is two-dimensional and turbulent. A simple Prandtl's mixing length model, for which the fluid viscosity is enhanced by turbulent mixing processes, is adopted.

Upon the foregoing assumptions, the partial differential equations governing the transport of mass, momentum and energy may then be formulated in terms of vorticity–stream function–temperature for a cartesian coordinate system. However, as melting proceeds, the solid/liquid interface moves to the right while being distorted by the uniform heat fluxes along its surface. As a result, the irregular time-changing shape of the solid/liquid interface will not necessarily coincide with grid nodes for a cartesian grid and attempts to solve the resulting finite-difference equations may lead to inaccurate or divergent solutions.

To overcome these difficulties, the governing equations are readily cast from their cartesian reference frame to a curvilinear reference frame (ξ, η). The advantage of this transformation is

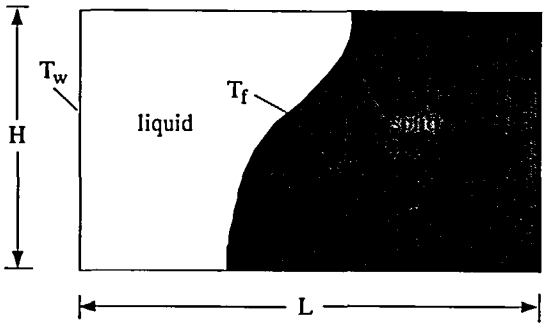

Figure 1 Schematic of the physical model

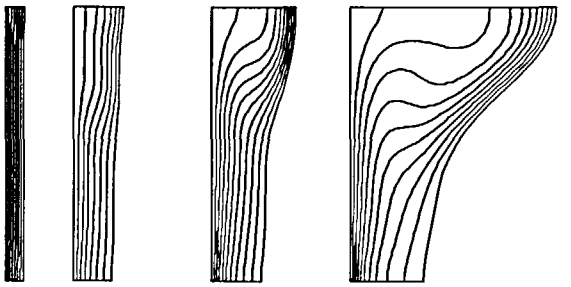

Figure 2 Isotherms for $Ra=10^6$ at $t=0.05, 0.1, 0.25$ and 1.5

the fact that, in the physical plane, boundary nodes always coincide with the distorted phase front. In the computational space (ξ,η), the boundary conditions are then specified on straight boundaries. Adopting this technique[5], the general dimensionless transport equation has the following form:

$$\frac{\partial(\rho\phi)}{\partial t}+\xi_t\frac{\partial(\rho\phi)}{\partial\xi}+\eta_t\frac{\partial(\rho\phi)}{\partial\eta}+\frac{\partial}{\partial\xi}\left(\rho U\phi-\left[\Gamma\left(g^{11}\frac{\partial(m\phi)}{\partial\xi}+g^{12}\frac{\partial(m\phi)}{\partial\eta}\right)\right]\right)+$$
$$\frac{\partial}{\partial\eta}\left(\rho V\phi-\left[\Gamma\left(g^{22}\frac{\partial(m\phi)}{\partial\eta}+g^{12}\frac{\partial(m\phi)}{\partial\xi}\right)\right]\right)=S(\xi,\eta) \quad (1)$$

where ϕ is the dependent variable, $S(\xi,\eta)$ is a source term, Γ is an exchange coefficient and ρ is a constant. These parameters are defined in *Table 1*.

The geometric coefficients U, V, g^{11}, g^{12}, g^{22}, g, ξ_t and η_t are defined as:

$$U=g\frac{\partial\psi}{\partial\eta} \qquad V=-g\frac{\partial\psi}{\partial\xi} \qquad g^{11}=\xi_x^2+\xi_y^2$$
$$g^{22}=\eta_x^2+\eta_y^2 \qquad g^{12}=\xi_x\eta_x+\xi_y\eta_y \qquad g=\xi_x\eta_y-\xi_y+\eta_x \quad (2)$$
$$\xi_t=-(\xi_x x_t+\xi_y y_t) \qquad \eta_t=-(\eta_x x_t+\eta_y y_t)$$

The initial conditions ($t=0$) are $\psi=\omega=\theta=0$. For $t>0$, the boundary conditions are given in *Table 2*. Furthermore, since no heat conduction occurs in the solid phase, all heat transferred to the interface is utilized for melting. Then an energy balance for the interface yields the following dimensionless condition for the moving boundary:

$$\frac{\partial x}{\partial t}=-\frac{Ste}{\tilde{\rho}}\left(\xi_x\frac{\partial\theta}{\partial\xi}+\eta_x\frac{\partial\theta}{\partial\eta}\right) \quad (3)$$

Ra, *Pr* and *Ste* represent the Rayleigh, Prandtl and Stefan numbers respectively, $\tilde{\rho}$ is the ratio

Table 1 Variables and parameters in equation (1)

Function	ϕ	ρ	Γ	m	$S(\xi,\eta)$
Stream function	ψ	0	1	1	ω
Variables:					
Vorticity	ω	1	1	$Pr+\varepsilon_M$	$Ra.Pr.\left(\xi_x\frac{\partial\theta}{\partial\xi}+\eta_x\frac{\partial\theta}{\partial\eta}\right)$
Temperature	θ	1	$1+\varepsilon_M/\varepsilon_H$	1	0

Table 2 Boundary conditions for the problem

Boundary	Stream function, ψ	Vorticity, ω	Temperature, θ
Left heated wall	$\psi=0$	$-g^{11}\dfrac{\partial^2\psi}{\partial\xi^2}$	$\theta=1$
Solid/liquid interface	$\psi=0$	$-g^{11}\dfrac{\partial^2\psi}{\partial\xi^2}$	$\theta=0$
Top and bottom walls	$\psi=0$	$-g^{22}\dfrac{\partial^2\psi}{\partial\eta^2}$	$\dfrac{\partial\theta}{\partial\eta}=-\dfrac{g^{12}}{g^{22}}\dfrac{\partial\theta}{\partial\xi}$

of the solid density to the liquid density. ε_M is the eddy viscosity which takes the following form in the (ξ,η) plane:

$$\varepsilon_M=l^2[g^{11}\psi_{\xi\xi}+2g^{12}\psi_{\xi\eta}+g^{22}\psi_{\eta\eta}+(\xi_{xx}+\xi_{yy})\psi_\xi+(\eta_{xx}+\eta_{yy})\psi_\eta]^{1/2} \tag{4}$$

where l is the Prandtl's mixing length. This mixing length is usually problem dependent and is determined empirically. Based on previous studies for turbulent flows inside cavities, this length was taken as $10^{-2}H$ and the ratio $\varepsilon_M/\varepsilon_H=0.9$. The authors recognize the limits of the present algebraic eddy-viscosity turbulence model. Nevertheless, this model was retained primarily for its simplicity and also for limiting the CPU time. However, in the future more sophisticated (and more realistic) turbulence models, such as the k–ε model[6], will be envisaged.

The finite difference equations are obtained on integrating the general governing equation (1) over each of the control volume in the (ξ,η) plane. The linearized equations are then solved interatively for θ, ω and ψ using an alternating line-by-line solver.

The overall numerical solution proceeds through a series of small time intervals during which the solid/liquid interface is assumed to be fixed. For each such interval, the field equations are solved by a fully implicit solution scheme (without neglecting the unsteady terms) in the new fixed domain. The solution of the field equations provides the energy fluxes at the interface after that time interval. The displacement of the interface can then be calculated explicitly from the interfacial energy balance (3) and a new solution domain is generated from the next time step.

The present model has been successfully validated through comparisons with experimental data and further details may be found in References 5, 7 and 8.

RESULTS AND DISCUSSION

The foregoing model was used for simulating turbulent natural convection melting of a pure metal from an isothermal wall. Following previous studies[5,7,8], the Prandtl and Stefan numbers were set to constant values of 0.02 and 0.042 respectively. These values are typical of a gallium melting system. The Rayleigh number ranged from 10^6 to 10^9.

To avoid computational difficulties at $t=0$, a very thin uniform thickness melt layer parallel to the heated wall was assumed to exist initially. The layer thickness was chosen such that the Rayleigh number based on this initial gap width was small enough so that pure conduction could be considered as the prevailing mechanism of heat transfer.

Following a grid refinement study and as a compromise between cost and accuracy, the calculations were done with a grid size 21×21 by non-uniformly distributed nodes. This makes it possible to concentrate several grid points in the critical regions near the heated wall and the solid/liquid interface where large temperature gradients prevail. The total simulated dimensionless melting time was 1.5 with a constant time step of 5×10^{-3}. The CPU time was approximately 12 hours on an IRIS 4D-60 (33 MHz). Most of the CPU time was spent on the vorticity equation as a very small relaxation parameter (~0.01) ought to be employed in order to avoid possible divergence of the numerical scheme.

Figure 2 shows the time evolution of the isotherms for $Ra=10^6$. Increments between isotherms are constant and equal to 0.1. The isotherm along the heated wall is $\theta=1.0$ and the isotherm along the solid/liquid interface is $\theta=0.0$. As expected, the solid/liquid interface, being an isotherm itself, always intersect the adiabatic top and bottom walls at right angles. At early times (0.05), heat transfer is predominated by conduction and the solid/liquid interface moves parallel to the vertical heated wall. After some time (0.1–0.25) convection appears and develops in the upper portion of the melt while conduction continues to prevail in the lower portion. Consequently, the interface exhibits a strong curvature in the upper portion and remains vertical in the lower portion.

As melting still progresses (1.5), the recirculating eddy in the upper half of the cavity grows in size enhancing even more the melting rates near the top of the cavity. This recirculating eddy is responsible for the higher temperature gradients near the top of the solid/liquid interface which account for the high melt velocity there. Comparison of the isotherm maps for various Rayleigh numbers (*Figure 3*) reveals that the local temperature gradient is substantially higher at higher Ra. Consequently, the local melt front velocity is highest for $Ra=10^9$.

The isotherm plots also illustrate that the boundary-layer regime has been established for all Rayleigh number calculations at the dimensionless time shown. This is indicated qualitatively by clustered vertical isotherms along the heated wall and melt front and horizontal isotherms in the core of the cavity. This Figure also shows the superimposed velocity vectors. Velocities at the centre of the stagnant core are very low compared to those in the boundary layers, differing by as much as an order of magnitude.

The time history of the local Nusselt number profile at the heated wall is shown in *Figure 4* for $Ra=10^6$ and $Ra=10^8$. Initially, in the conduction regime for $Ra=10^6$, the Nusselt number is uniform over most of the heated wall (0.05). At the same time for $Ra=10^8$, however, the convection regime has already superseded the conduction regime. As time passes, the melt cavity expands and the thermal resistance across the liquid layer increases. This results in a general decrease in the magnitude of the local Nusselt number. For $Ra=10^6$, at $t=0.25$, there is a plateau of locally high Nusselt number in the centre region of the heated wall. This region can be correlated to the height of the knee on the solid/liquid interface. Cold fluid from the melt front joining the boundary layer on the hot wall creates a region of locally higher heat transfer at the knee of the interface. As time progresses (1.5), the melt cavity becomes so large that the

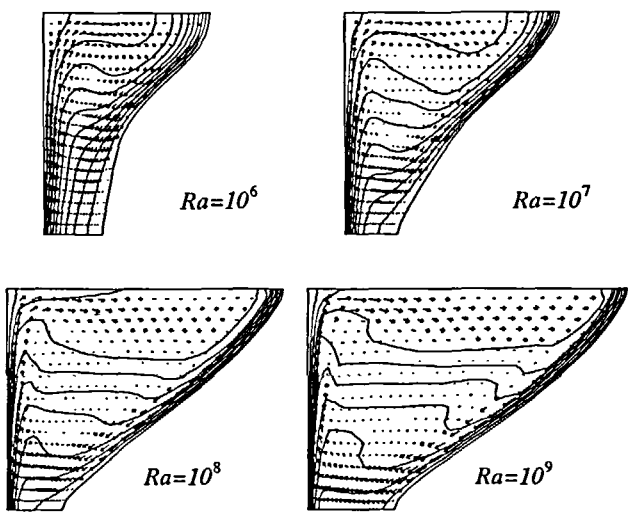

Figure 3 Velocity vector maps and isotherms at $t=1.5$

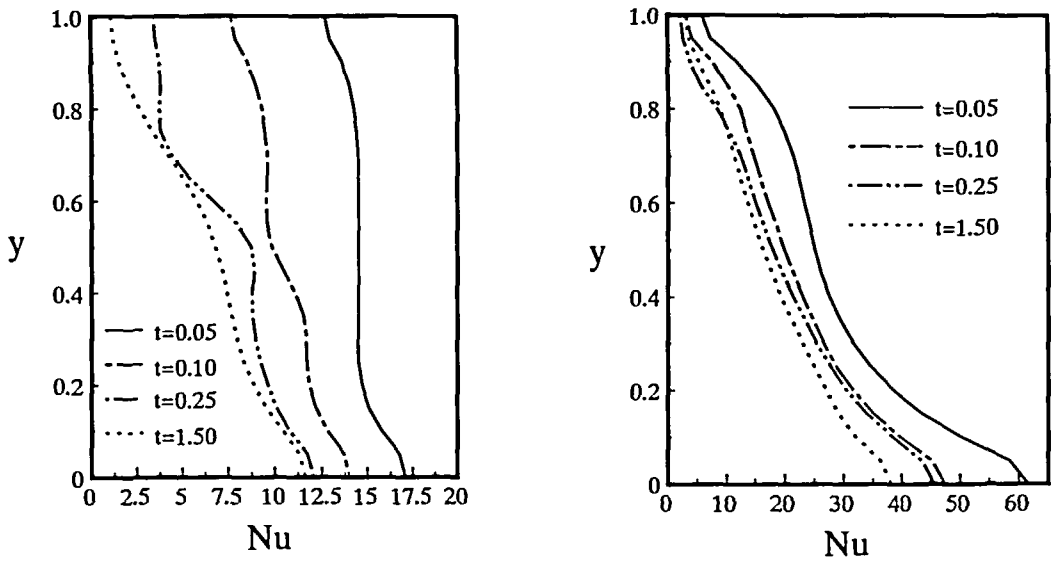

Figure 4 Local Nusselt numbers at the heated wall for $Ra=10^6$ and $Ra=10^8$

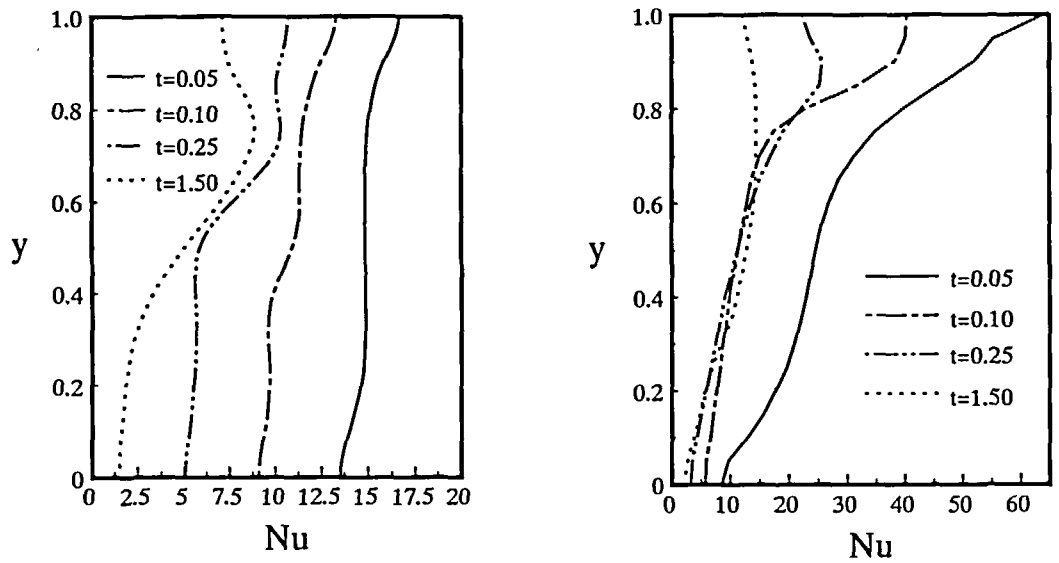

Figure 5 Local Nusselt numbers at the solid/liquid interface for $Ra=10^6$ and $Ra=10^8$

knee on the melting front no longer has a strong local influence on the energy transport at the heated wall and the plateau of high Nu is suppressed. For larger Ra, the same behaviour was observed but at earlier times as the convective flow is stronger.

Figure 5 illustrates the local Nusselt number profiles at the solid/liquid interface corresponding to those of *Figure 4*. The Nusselt number at the melting front is calculated from the normal temperature gradient $\nabla\theta.\vec{n}$ along the interface contour. Again, the Nusselt number for $Ra=10^6$

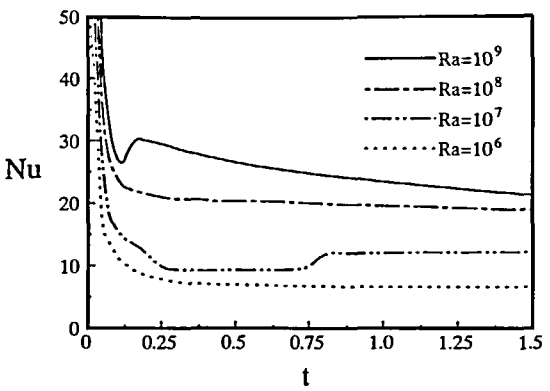

Figure 6 Temporal variation of the average Nusselt number at the heated wall

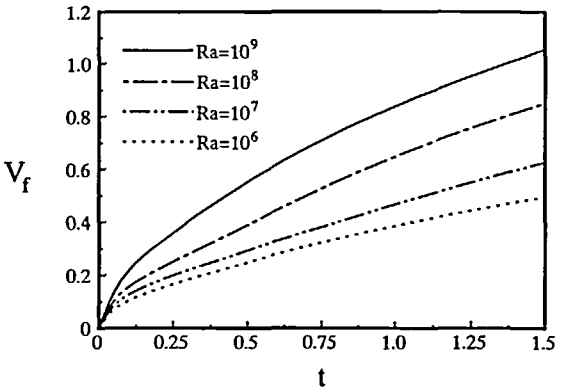

Figure 7 Temporal variation of the molten volume fractions for all cases

is seen to be nearly uniform initially (0.05) and deviates with the onset of buoyancy-induced fluid motion. For $Ra=10^8$, the convective flow has already established itself at 0.05. The heat transfer is highest near the top of the phase front where hot fluid impinges. For larger *Ra* number, the Nusselt number is obviously larger. The magnitude of the local Nusselt number also decreases with time. Interestingly enough, the plateau of locally high Nusselt number for $Ra=10^6$, at $t=0.25$ may also be observed at the phase front.

The average Nusselt number at the heated wall was also calculated from the converged temperature field for each time step in the melting process. This is shown in *Figure 6*. As expected, higher Rayleigh numbers result in an earlier departure form the pure conduction behaviour. A higher *Ra* also leads to a higher $\overline{Nu}$ in the quasi-steady melting regime. In fact, the average Nusselt number changes very little with time in the quasi-steady melting regime after the natural convective flow is well established. It was correlated, in this regime, for all Rayleigh numbers studied according to the following equation:

$$\overline{Nu}=1.75Ra^{0.12} \tag{5}$$

This correlation for turbulent natural convection melting is quite different form those obtained experimentally and numerically for laminar natural convection melting[3–5]. For the latter, the heated-wall Nusselt number exhibits dependences of $Ra^{0.26}$.

Finally, the temporal variation of the molten volume fraction was determined and is depicted in *Figure 7*. As for laminar convective flows, the V_f *versus* t relationship for turbulent flows is almost linear in the quasi-steady melting regime.

CONCLUSIONS

Melting of a low Prandtl number substance with turbulent natural convection in the melt has been studied analytically. Results indicate that turbulent flow increases the overall heat transfer and melting rates. The average heated-wall Nusselt number exhibits dependences of $Ra^{0.12}$ markedly different from those for laminar flows.

ACKNOWLEDGEMENTS

The authors are very grateful to the National Science and Engineering Research Council of Canada for their financial support of this work.

REFERENCES

1 Gau, C. amd Viskanta, R. Melting and solidification of a pure metal on a vertical wall, *ASME J. Heat Transfer*, **108**, 174–181 (1986)
2 Morgan, K. A numerical analysis of freezing and melting with convection, *Comp. Meth. Appl. Mech. Eng.*, **28**, 275–284 (1981)
3 Webb, B. W. and Viskanta, R. Analysis of heat transfer during melting of a pure metal from an isothermal vertical wall, *Num. Heat Transfer*, **5**, 539–558 (1984)
4 Brent, A. D., Voller, V. R. and Reid, K. J. Enthalpy–porosity technique for modelling convection–diffusion phase change: application to the melting of a pure metal, *Num. Heat Transfer*, **13**, 297–318 (1988)
5 Lacroix, M. Computation of heat transfer during melting of a pure substance form an isothermal wall, *Num. Heat Transfer*, **15**, 191–210 (1989)
6 Launder, B. E. and Spalding, D. B. *Mathematical Models of Turbulence*, Academic Press, London (1972)
7 Lacroix, M. and Voller, V. Finite difference solutions of solidification phase change problems: transformed *versus* fixed grids, *Num. Heat Transfer*, (*B*), **17**, 25–41 (1990)
8 Lacroix, M. and Garon, A. Numerical solutions of phase change problems: an Eulerian–Lagrangian approach, *Num. Heat Transfer*, (*B*), **19**, 57–78 (1991)